COMMUNICATION

Effect of Block Copolymer Architecture and Composition on Gold Nanoparticle Fabrication

Received 00th January 20xx,
Accepted 00th January 20xx

DOI: 10.1039/x0xx00000x

Anna P. Constantinou, Uriel Marie-Sainte, Lihui Peng, Dean R. Carroll, Catriona M. McGilvery, Iain E. Dunlop* and Theoni K. Georgiou*

Gold nanoparticles (AuNPs) have many biomedical applications. Their size is a crucial parameter, as it affects cellular uptake. Here, we investigate how the formation of AuNPs is affected by the composition and architecture (AB, BAB and ABA) of the copolymers, which were used as templates for the fabrication of AuNPs.

Gold nanoparticles (AuNPs) have been extensively studied over the past two decades due to their electronic, optical and catalytic properties.[1-3] In medicine, their ability to be used as imaging agents for diagnosis and photothermal therapy has made AuNPs particularly attractive.[1,3-9] While the most common approach has been to synthesise AuNPs using small-molecule surfactants such as citrate,[10-12] this inevitably leads to a multistep process, since inorganic nanoparticles for biomedical applications require a brush-like coating of an antifouling polymer such as poly(ethylene glycol) (PEG) to stabilise them and eliminate non-specific interactions with proteins and cells.[13,14] There is thus growing interest in the alternative approach of synthesising AuNPs within the core of polymeric precursors,[1,2,15-17] e.g. pre-existing polymer micelles,[1,2,15] so that a PEGylated nanoparticle construct is generated directly without the need for a subsequent PEGylation step.[1,2] The overall size and shape of this PEGylated AuNP construct is of the foremost importance as it affects the biofunctional properties of the particles, resulting in e.g. different cellular uptake times.[18-20] Thus, tuning the size and the shape of the AuNP-polymer construct is crucial in designing effective diagnostic and therapeutic tools.[21-23] Furthermore, the incorporation of additional functional groups into the stabilising PEG corona can manipulate surface charge and provide a platform on which targeting moieties for specific cell types can be attached; the latter is known as active targeting.[24]

In this study, we have chosen to fabricate AuNPs within the cores of micelles produced by well-defined block copolymers, using amine groups to promote the *in-situ* reduction of $HAuCl_4$.[25-29] Specifically, when the $HAuCl_4$ reacts with the amine groups, Au^{3+} is reduced to Au^0, while the amine groups (NR_3) are oxidised to $NR^{3+\cdot}$.[25] The simplicity of this method is advantageous, as it eliminates the requirement of additional reducing reagents, which would need to be removed later. The AuNP is formed in the core of the micelle, where it likely complexes the amine-groups. Here, we report the fabrication of AuNPs using copolymers of varying architectures and compositions, which are based on 2-(diethylamino)ethyl methacrylate (DEAEMA, A block), an amine-containing monomer that becomes hydrophobic when deprotonated at higher pH values, and which will form the micelle core and poly(ethylene glycol) methyl ether methacrylate (PEGMA, B block), which is hydrophilic and it will form the corona.

To the best of our knowledge this is the first study in which polymers of different architectures have been systematically tested in the fabrication of AuNPs. Specifically, AB diblock, and ABA and BAB triblock copolymers have been synthesised to investigate how the architecture affects the fabrication and size of the AuNPs. For the AB and BAB architectures, we have varied the composition of the polymer to systematically alter the relative amounts of DEAEMA and PEGMA. The polymers were synthesised by group transfer polymerisation (GTP),[30-32] a living polymerisation method that enables the synthesis of well-defined polymers,[33] i.e. polymers with defined molar mass (MM), architecture and composition. DEAEMA has been chosen as the hydrophobic amine-containing monomer that will form micelle cores, while PEGMA has been chosen to generate a hydrophilic anti-fouling corona of PEG around the micelle core, and later around the nanoparticle. Propargyl methacrylate (PMA) groups have also been incorporated into the PEGMA based blocks to enable post-polymerisation functionalisation, such click chemistry to attach imaging or targeting moieties.[34,35]

The synthesis of the polymers was performed via an one-pot, sequential GTP, similarly to previous reports.[34,36-50] The

[a] *Department of Materials, Exhibition Road, Royal School of Mines, Imperial College London, SW7 2AZ, UK. E-mail: i.dunlop@imperial.ac.uk and t.georgiou@imperial.ac.uk .*

† Footnotes relating to the title and/or authors should appear here.
Electronic Supplementary Information (ESI) available: [details of any supplementary information available should be included here]. See DOI: 10.1039/x0xx00000x

successful synthesis of the polymers was confirmed with gel permeation chromatography (GPC) and proton nuclear magnetic resonance (NMR) spectroscopy. The resulting polymer's MM, dispersity indices (*Đ*) and comonomer (PEGMA and DEAEMA) compositions are shown in Table 1. A more detailed report of the polymer synthesis can be found in the Supporting Information in Table S1. In total, 7 polymers were synthesised, specifically three BAB (where B = PEGMA and A = DEAEMA) and three AB block copolymers of varying comonomer composition and one ABA triblock copolymer. All synthesised copolymers presented *Đ* lower than 1.25, which is satisfactory and expected for macromonomer-based GTP-synthesised polymers.[37,38,41,43,51,52]

The polymers are schematically illustrated in Figure 1. The expectation is that the BAB triblocks and AB diblocks will both assemble into classical spherical micelles with a PEG corona as illustrated schematically in Figure 2 (a). The ABA triblock on the other hand is expected to form flower micelles, as shown schematically in Figure 2 (b).

The 1 w/w% aqueous solutions of the copolymers were characterised to determine the polymers' pK_a and cloud point (CP). The results are displayed in Table 2. It can be clearly observed that both the polymer's pK_a and CP decreased as the content in the hydrophobic DEAEMA increased. Specifically, the pK_as decreased from 7.1 to 6.8 for both BAB and AB diblock copolymers as the hydrophobic content increased. This trend has been observed previously, and it is attributed to the decreased dielectric constant by increasing hydrophobicity.[37,38,40,43,51,53] The CPs decreased from 61 to 57 °C for both BAB and AB diblock copolymers as the hydrophobic content increased, as expected and observed before.[37,38,40,41,43,54,55] It is interesting to point out that neither the pK_a nor the CP were affected by the polymer architecture, as polymers with the same DEAEMA content, but different architecture, presented the same pK_as and CPs within the experimental error. The titration curves can be found in Figure S3 in the SI.

Table 1: MMs, dispersities and composition of the synthesised polymers.

No.	Architecture	Theoretical Polymer Structure	M_n (g mol^{-1}) [a]	*Đ* [a]	DEAEMA-PEGMA-PMA (w/w%)	
					Theoretical	Experimental [b]
P1	BAB	$PEGMA_{14}$-*b*-$DEAEMA_{19}$-*b*-$PEGMA_{14}$-*b*-PMA_2	17400	1.19	29-69-2	29-70-1
P2		$PEGMA_{12}$-*b*-$DEAEMA_{26}$-*b*-$PEGMA_{12}$-*b*-PMA_2	15400	1.20	39-59-2	38-60-2
P3		$PEGMA_{10}$-*b*-$DEAEMA_{32}$-*b*-$PEGMA_{10}$-*b*-PMA_2	17100	1.19	49-49-2	46-52-2
P4	AB	$DEAEMA_{19}$-*b*-$PEGMA_{28}$-*b*-PMA_2	14700	1.20	29-69-2	26-72-2
P5		$DEAEMA_{26}$-*b*-$PEGMA_{24}$-*b*-PMA_2	16500	1.17	39-59-2	37-61-2
P6		$DEAEMA_{32}$-*b*-$PEGMA_{20}$-*b*-PMA_2	16400	1.12	49-49-2	48-50-2
P7	ABA	$DEAEMA_{10}$-*b*-($PEGMA_{28}$-*co*-PMA_2)-*b*-$DEAEMA_{10}$	13900	1.29	29-69-2	27-71-2

[a] These values were determined by GPC analysis before precipitation.
[b] These values were determined by ^{1}H NMR analysis after precipitation.

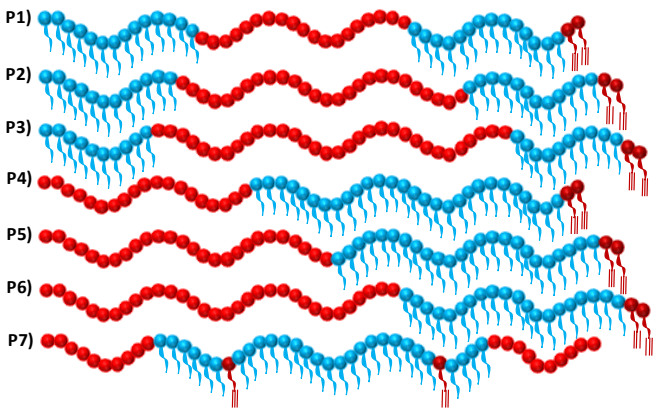

Figure 2: Schematic representation of the different polymer investigated in this study. The PEGMA, DEAEMA and PMA units are shown in blue, red, and dark red spheres, respectively.

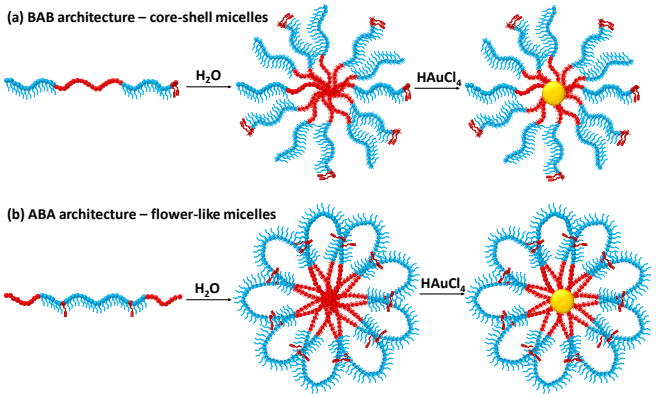

Figure 1: Schematic illustration of the self-assembly behaviour of (a) Polymer 1, which is a BAB triblock copolymer with the hydrophobic part in the centre of the polymer chain, and (b) Polymer 7, which is an ABA triblock copolymer with the hydrophilic part in the part in the centre of the polymer chain. The subsequent formation of AuNPs by the addition of $HAuCl_4$ is also presented. The PEGMA, DEAEMA and PMA units are show in blue, red and dark red spheres, respectively.

Table 2: Diameter size of the micelles, pK_a and cloud points of the synthesised polymers in DI water at initial pH (pH ≈ 8).

No.	Architecture	DEAEMA:PEGMA (w/w%)	Theoretical Polymer Structure	pK_a ± 0.1	Diameter / nm		Cloud Point ± 0.1 / ˚C
					Theoretical	By DLS*	
P1	BAB	29:70	PEGMA$_{14}$-*b*-DEAEMA$_{19}$-*b*-PEGMA$_{14}$-*b*-PMA$_2$	7.0	21 [a]	13.5	61
P2		38:60	PEGMA$_{12}$-*b*-DEAEMA$_{26}$-*b*-PEGMA$_{12}$-*b*-PMA$_2$	7.0	20 [a]	11.7	59
P3		46:52	PEGMA$_{10}$-*b*-DEAEMA$_{32}$-*b*-PEGMA$_{10}$-*b*-PMA$_2$	6.8	26 [a]	11.7	57
P4	AB	26:72	DEAEMA$_{19}$-*b*-PEGMA$_{28}$-*b*-PMA$_2$	7.1	32 [b]	21.0	61
P5		37:61	DEAEMA$_{26}$-*b*-PEGMA$_{24}$-*b*-PMA$_2$	6.9	32 [b]	21.0	60
P6		48:50	DEAEMA$_{32}$-*b*-PEGMA$_{20}$-*b*-PMA$_2$	6.8	22 [b]	24.4	57
P7	ABA	27:71	DEAEMA$_{10}$-*b*-(PEGMA$_{28}$-*co*-PMA$_2$)-*b*-DEAEMA$_{10}$	7.1	19 [c]	18.2	62

[a] For the BAB architecture, the theoretical diameter was calculated as follows: (DP_A+DP_B+2*DP_C)*0.254nm.
[b] For the AB architecture, the theoretical diameter was calculated using the following equation: (DP_A+2*DP_B+2*DP_C)*0.254nm.
[c] for the ABA architecture, the theoretical diameter of the flower-like micelle was calculated by the following equation: (DP_A+DP_B+DP_C)*0.254nm.
Note: In the equations mentioned above, DP stands for degree of polymerisation, which were calculated by using the results by GPC and ^{1}H NMR analysis, whereas A, B, and C are DEAEMA, PEGMA, and PMA, respectively. The value of 0.254nm is the projected length of one methacrylate repeated unit.
* The results reported are the ones corresponding to the maximum of the peak by intensity. In case more than one peak is present, the value reported corresponds to the maximum of the highest intensity peak. Complete DLS results can be found in Figure S2.

The self-assembly into micelles of 1 w/w% aqueous copolymer solutions has also been shown. The micelles' diameter was strongly affected by the architecture of the copolymers, while no specific trend was observed in terms of the comonomer composition. As can be seen in Table 2, smaller micelles were formed by the BAB architecture, compared to the AB architecture, as expected. The theoretical calculations of the diameters, presented in Table 2, assume: i) the DEAEMA block is hydrophobic and forms the core of the micelle, regardless the pH, ii) the hydrophobic part fully overlaps, iii) the methacrylate backbone is fully extended, and iv) the ABA triblock copolymer is expected to form flower micelles, in which all the polymer chains fold in a pedal-shape. The experimental diameters are generally smaller than the corresponding theoretical ones, since the theoretical calculations assume that the polymer chains are fully extended, as mentioned above. However, Polymer 6, which is an AB diblock copolymer with the highest content in DEAEMA, forms slightly bigger micelles than the theoretical value, which can be explained by taking into consideration that incomplete overlap of the DEAEMA block might take place. It is interesting to note that the ABA triblock copolymer at initial pH (0% protonation of the amino units, pH ≈ 8) forms monodisperse micelles, without any unimers or larger aggregates present, as opposed to pH 7 (this is discussed in the following paragraphs).

All polymers were tested in terms of their ability to form and stabilise AuNPs. We have previously shown on a related system that nanoparticle formation is optimal at a pH in the vicinity of the amine pK_a point (here around pH 7).[27] This may be attributed to the fact that amine-induced reduction of gold (III) chloride requires liberation of H^+ which is disfavoured at low pH,[25] but at very high pH the micelle core may be too hydrophobic for the gold (III) chloride to infiltrate it. Hence, all particles were fabricated at pH 7, with polymer and gold solutions separately adjusted to this value before synthesis. Different $HAuCl_4$ to DEAEMA molar ratios were tested as follows: 0.3, 0.5 and 0.7. Table 3 lists the diameters of the AuNP-polymer constructs when 0.5 $HAuCl_4$:DEAEMA was used, determined by dynamic light scattering (DLS), and the diameters of the corresponding micelles prior to mixing with gold (III) chloride. Note that the nanoparticle diameters quoted are the hydrodynamic diameters of the entire gold-polymer construct. Particle formation was monitored over time using UV-visible spectroscopy and the results are presented in Figure 3. The growth initiation time (Table 3) is taken as the point at which absorbance at 520 nm becomes greater than 2.

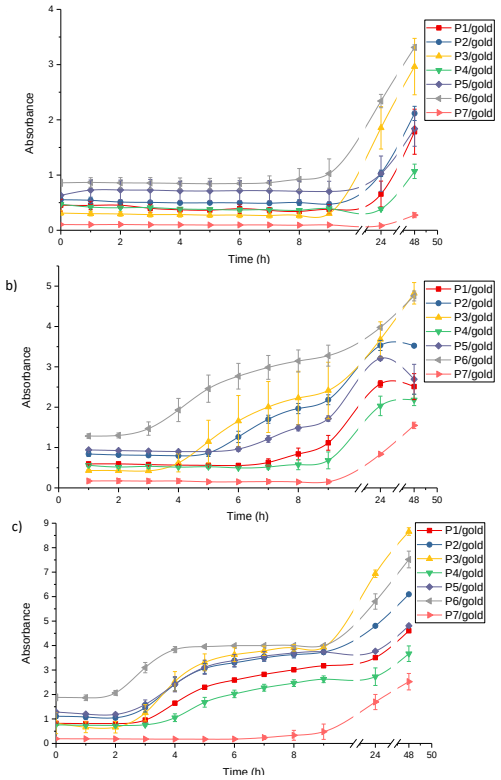

Figure 3: Graphs showing the kinetics of solutions containing different polymers mixed with gold at certain $HAuCl_4$:DEAEMA molar ratio. The graphs show the evolution of the absorbance at a 520 nm wavelength over time. a) Molar ratio 0.3 b) Molar ratio 0.5 c) Molar ratio 0.7.

Table 3: Diameter size of the micelles and the polymer/gold particles (0.5 molar ratio of $HAuCl_4$ to DEAEMA) at pH 7.

No.	Architecture	DEAEMA:PEGMA (w/w%)	Theoretical Polymer Structure	DLS results		Particle diameter ± Std Error / nm [b]	Growth initiation time / hrs
				Micelle diameter / nm [a]	PDI		
P1	BAB	29:70	$PEGMA_{14}$-*b*-$DEAEMA_{19}$-*b*-$PEGMA_{14}$-*b*-PMA_2	13.5	1.000	31 ± 3	9<t<24
P2		38:60	$PEGMA_{12}$-*b*-$DEAEMA_{26}$-*b*-$PEGMA_{12}$-*b*-PMA_2	18.2	0.262	31 ± 3	7
P3		46:52	$PEGMA_{10}$-*b*-$DEAEMA_{32}$-*b*-$PEGMA_{10}$-*b*-PMA_2	13.5	0.139	31 ± 3	6
P4	AB	26:72	$DEAEMA_{19}$-*b*-$PEGMA_{28}$-*b*-PMA_2	24.4	0.416	33 ± 1	9<t<24
P5		37:61	$DEAEMA_{26}$-*b*-$PEGMA_{24}$-*b*-PMA_2	21.0	0.066	28 ± 1	9
P6		48:50	$DEAEMA_{32}$-*b*-$PEGMA_{20}$-*b*-PMA_2	28.2	0.114	39 ± 6	3
P7	ABA	27:71	$DEAEMA_{10}$-*b*-($PEGMA_{28}$-*co*-PMA_2)-*b*-$DEAEMA_{10}$	18.2	0.722	31 ± 3	9<t<24

[a] The results reported are the ones corresponding to the maximum of the peak by intensity. In case more than one peak is present, the diameter reported is the one corresponding to the maximum of the micelles peak. Complete DLS results can be found in Figure S2.
[b] The experiment was repeated twice, thus the value reported is the average diameter. The diameter corresponding to the maximum of the peak was used for the calculations. Complete DLS results can be found in Figure S2.

To characterise the gold core of the nanoparticles, we have selected one example of each architecture for detailed characterisation by synchrotron small-angle X-ray scattering (SAXS); specifically, Polymer 3 as an example of BAB, Polymer 6 as an example of AB and Polymer 7 as an example of ABA. In all cases SAXS showed that the gold cores were spherical, with diameters in the 8-10 nm range and a population Gaussian dispersity in the range 0.20-0.25 (i.e. the standard deviation normalized by the mean (Figure S7, Tables S3, S4). Hence the gold core diameter is roughly 1/3 of the micelle diameter with no difference in this case between the three different architectures. The spherical nature of the particle gold cores was further confirmed by transmission electron microscopy (TEM) (Figure S6).

Returning to the overall diameter of the gold-micelle construct, in most of the cases, it is observed that the size of these particles is higher than the corresponding micelles, as expected, since the Au was incorporated in the centre of the micelles.

Interestingly, the architecture and the composition of the copolymers influence the time that the particles need to be formed, as well as the size of the particles. In summary five main observations can be made:

(i) All the copolymers with the lowest hydrophobic amino content, regardless the architecture, form micelles with significant population of unimers and/or aggregates, as indicated by the high polydispersity (PDI) values. As a result, the particles formed by these copolymers need more time to be formed.

(ii) Concerning copolymers of the same architecture, either BAB or AB, the time needed for particle formation is shorter as the hydrophobic amino content increases. This shows the important role of the amino groups on the synthesis of AuNPs.

(iii) For the BAB triblock copolymers, there is no significant difference in the particle size, regardless of the change in composition. However, similarly to the AB diblock copolymers, the higher the DEAEMA:PEGMA ratio, the faster the AuNPs are formed.

(iv) The ABA architecture, which adopts flower-like micelle configuration, forms AuNPs of a comparable size as the BAB architectures, regardless the composition.

(v) Polymer 6, which is the AB diblock copolymer with the highest hydrophobic amino content, forms mostly micelles with no significant population of unimers or large aggregates (as indicated by the low PDI value). Polymer 6 also forms particles faster than all the other polymers.

In conclusion, it has been demonstrated that both the polymer composition and block position (architecture) influence the formation and the size of the AuNPs. Most importantly, the AB diblock copolymer with the highest content in the hydrophobic amino unit forms mostly micelles (no unimers or large aggregates are present) and it is the best-performing in terms of fabrication of AuNPs with this micelle-templating method. The absence of unimers and large aggregates is confirmed by the presence of only species with size corresponding to micelles, as proved by DLS (Table S2). Therefore, a set of polymer structure criteria and conditions for AuNPs synthesis have been determined, which are important in designing and tailoring AuNPs for biomedical applications.

Acknowledgments

This project was supported by an EPSRC Doctoral Prize Fellowship to APC, and by the Diamond Light Source Ltd. SAXS measurements were performed by Mr Nikul Khunti (Diamond, Mail-in Experimental Session SM21035-42).

Conflicts of interest

The authors declare no conflicts of interest.

References

1 J. Shan and H. Tenhu, *Chem. Commun.,* 2007, 4580-4598.
2 P. Alexandridis, *Chem. Eng. Technol.,* 2011, **34**, 15-28.

3 M. S. Bakshi, *Advances in Colloid and Interface Science,* 2014, **213**, 1-20.
4 M. Daniel and D. Astruc, *Chem. Rev.,* 2004, **104**, 293-346.
5 X. Yang, M. Yang, B. Pang, M. Vara and Y. Xia, *Chem. Rev.,* 2015, **115**, 10410-10488.
6 J. Chen, F. Saeki, B. J. Wiley, H. Cang, M. J. Cobb, Z. Li, L. Au, H. Zhang, M. B. Kimmey, Li and Y. Xia, *Nano Lett.,* 2005, **5**, 473-477.
7 C. J. Lin, T. Yang, C. Lee, S. H. Huang, R. A. Sperling, M. Zanella, J. K. Li, J. Shen, H. Wang, H. Yeh, W. J. Parak and W. H. Chang, *ACS Nano,* 2009, **3**, 395-401.
8 Y. Zhang, X. Zhan, J. Xiong, S. Peng, W. Huang, R. Joshi, Y. Cai, Y. Liu, R. Li, K. Yuan, N. Zhou and W. Min, *Scientific Reports,* 2018, **8**, 8720.
9 S. Bharathiraja, N. Q. Bui, P. Manivasagan, M. S. Moorthy, S. Mondal, H. Seo, N. T. Phuoc, T. T. Vy Phan, H. Kim, K. D. Lee and J. Oh, *Scientific Reports,* 2018, **8**, 500.
10 J. Turkevich, P. C. Stevenson and J. Hillier, *Discuss. Faraday Soc.,* 1951, **11**, 55-75.
11 S. Kumar, K. S. Gandhi and R. Kumar, *Ind Eng Chem Res,* 2007, **46**, 3128-3136.
12 J. Lee, H. Zhou and J. Lee, *J. Mater. Chem.,* 2011, **21**, 16935-16942.
13 E. S. Place, J. H. George, C. K. Williams and M. M. Stevens, *Chem. Soc. Rev.,* 2009, **38**, 1139-1151.
14 T. K. Georgiou, M. Vamvakaki, L. A. Phylactou and C. S. Patrickios, *Biomacromolecules,* 2005, **6**, 2990-2997.
15 E. Seo, S. Lee, S. Lee, S. Choi, C. J. Hawker and B. Kim, *Polym. Chem.,* 2017, **8**, 4528-4537.
16 N. Li, T. Tsoi, W. Lo, Y. Gu, H. Wan and W. Wong, *Polym. Chem.,* 2017, **8**, 6989-6996.
17 F. Wei, X. Cai, J. Nie, F. Wang, C. Lu, G. Yang, Z. Chen, C. Ma and Y. Zhang, *Polym. Chem.,* 2018, **9**, 3832-3839.
18 Arnida, A. Malugin and H. Ghandehari, *J. Appl. Toxicol.,* 2010, **30**, 212-217.
19 B. D. Chithrani, A. A. Ghazani and W. C. W. Chan, *Nano Lett.,* 2006, **6**, 662-668.
20 E. Oh, J. B. Delehanty, K. E. Sapsford, K. Susumu, R. Goswami, J. Blanco-Canosa, P. E. Dawson, J. Granek, M. Shoff, Q. Zhang, P. L. Goering, A. Huston and I. L. Medintz, *ACS Nano,* 2011, **5**, 6434-6448.
21 H. T. Ta, N. P. Truong, A. K. Whittaker, T. P. Davis and K. Peter, *Expert Opinion on Drug Delivery,* 2018, **15**, 33-45.
22 S. Y. Khor, M. N. Vu, E. H. Pilkington, A. P. R. Johnston, M. R. Whittaker, J. F. Quinn, N. P. Truong and T. P. Davis, *Small,* 2018, **14**, 1801702.
23 J. Zhao and M. H. Stenzel, *Polym. Chem.,* 2018, **9**, 259-272.
24 S. T. Jahan, S. M. A. Sadat, M. Walliser and A. Haddadi, *Journal of Drug Delivery,* 2017, **2017**, 1-24.
25 J. D. S. Newman and G. J. Blanchard, *Langmuir,* 2006, **22**, 5882-5887.
26 T. Ishii, H. Otsuka, K. Kataoka and Y. Nagasaki, *Langmuir,* 2004, **20**, 561-564.
27 I. E. Dunlop, M. P. Ryan, A. E. Goode, C. Schuster, N. J. Terrill and J. V. M. Weaver, *RSC Adv.,* 2014, **4**, 27702-27707.
28 S. Liu, J. V. M. Weaver, M. Save and S. P. Armes, *Langmuir,* 2002, **18**, 8350-8357.
29 L. Podhorska, D. Delcassian, A. E. Goode, M. Agyei, D. W. McComb, M. P. Ryan and I. E. Dunlop, *Langmuir,* 2016, **32**, 9216-9222.
30 O. W. Webster, W. R. Hertler, D. Y. Sogah, W. B. Farnham and T. V. RajanBabu, *J. Am. Chem. Soc.,* 1983, **105**, 5706-5708.
31 O. W. Webster, *J. Polym. Sci. Part A,* 2000, **38**, 2855-2860.
32 O. W. Webster, in *New Synthetic Methods*, Springer Berlin Heidelberg, Berlin, Heidelberg, 2004, p. 1-34.
33 O. W. Webster, *Science,* 1991, **251**, 887-893.
34 N. Ghasdian, M. A. Ward and T. K. Georgiou, *Chem. Commun.,* 2014, **50**, 7114-7116.
35 G. Luongo, P. Campagnolo, J. E. Perez, J. Kosel, T. K. Georgiou, A. Regoutz, D. J. Payne, M. M. Stevens, M. P. Ryan, A. E. Porter and I. E. Dunlop, *ACS Appl. Mater. Interfaces,* 2017, **9**, 40059-40069.
36 N. H. Raduan, T. S. Horozov and T. K. Georgiou, *Soft Matter,* 2010, **6**, 2321-2329.
37 M. A. Ward and T. K. Georgiou, *J. Polym. Sci. A Polym. Chem.,* 2010, **48**, 775-783.
38 M. A. Ward and T. K. Georgiou, *Soft Matter,* 2012, **8**, 2737-2745.
39 D. M. Buzza, P. D. I. Fletcher, T. K. Georgiou and N. Ghasdian, *Langmuir,* 2013, **29**, 14804-14814.
40 M. A. Ward and T. K. Georgiou, *J. Polym. Sci. Part A: Polym. Chem.,* 2013, **51**, 2850-2859.
41 M. A. Ward and T. K. Georgiou, *Polym. Chem.,* 2013, **4**, 1893-1902.
42 F. D. Fleischli, N. Ghasdian, T. K. Georgiou and N. Stingelin, *J. Mater. Chem. C,* 2015, **3**, 2065-2071.
43 A. P. Constantinou and T. K. Georgiou, *Polym. Chem.,* 2016, **7**, 2045-2056.
44 D. R. Carroll, A. P. Constantinou, N. Stingelin and T. K. Georgiou, *Polym. Chem.,* 2018, **9**, 3450-3454.
45 Stella C. Hadjiyannakou, Maria Vamvakaki and Costas S. Patrickios. 2004, **45**, 3681-3692.
46 N. A. Hadjiantoniou, A. I. Triftaridou, D. Kafouris, M. Gradzielski and C. S. Patrickios, *Macromolecules,* 2009, **42**, 5492-5498.
47 Eleni Kassi, Michalis S. Constantinou and Costas S. Patrickios. 2013, **49**, 761-767.
48 M. Rikkou-Kalourkoti, P. A. Panteli and C. S. Patrickios, *Polym. Chem.,* 2014, **5**, 4339-4347.
49 M. Elladiou and C. S. Patrickios, *Macromolecules,* 2015, **48**, 7503-7512.
50 P. A. Constantinou, Hanyi Zhao, M. C. McGilvery, E. A. Porter and K. T. Georgiou. 2017, **9**.
51 T. K. Georgiou, C. S. Patrickios, P. W. Groh and B. Iván, *Macromolecules,* 2007, **40**, 2335-2343.
52 G. Kali, T. K. Georgiou, B. Iván and C. S. Patrickios, *J. Polym. Sci. A Polym. Chem.,* 2009, **47**, 4289-4301.
53 O. E. Philippova, D. Hourdet, R. Audebert and A. R. Khokhlov, *Macromolecules,* 1997, **30**, 8278-8285.
54 A. I. Triftaridou, S. C. Hadjiyannakou, M. Vamvakaki and C. S. Patrickios, *Macromolecules,* 2002, **35**, 2506-2513.
55 A. P. Constantinou, N. Sam-Soon, D. R. Carroll and T. K. Georgiou, *Macromolecules,* 2018, **51**, 7019-7031.